Ultra high sensitivity, wideband Fabry Perot ultrasound sensors as an alternative to piezoelectric PVDF transducers for biomedical photoacoustic detection

Edward Z. Zhang* and Paul Beard
Department of Medical Physics and Bioengineering, University College London
Shropshire House, 11-20 Capper Street, London WC1E 6JA

ABSTRACT

A high sensitivity, wideband ultrasound sensor based on a high finesse Fabry-Perot (FP) polymer film interferometer has been demonstrated with a bandwidth of 20 MHz and a 50µm diameter active area. Used in conjunction with a balanced photodetector to enable the use of a high intensity interrogating light beam of up to 36mW, the sensor system provided a noise equivalent pressure (NEP) of 0.35kPa over a 20 MHz measured bandwidth. It is shown further that this NEP could, in principle, be reduced to 0.16 kPa by using an interrogating source with a wider wavelength tuning range than was available in the current study to track drift in the phase bias of the FP sensor. The sensitivity achieved is an order of magnitude higher than previously demonstrated with this type of sensors, and is comparable to that of a 1mm diameter PVDF element. The combination of high sensitivity and the small active area (<50µm diameter) makes the FP sensor scheme particularly suitable for photoacoustic imaging applications.

Keywords: Photoacoustic, ultrasound array, biomedical, photodetector, Fabry Perot sensor, PVDF transducer

1. INTRODUCTION

Photoacoustic imaging is a new broadly applicable method of non-invasive medical imaging, for visualizing the internal structure and function of soft tissues. Applications including imaging the breast for the diagnosis and screening of cancer [1, 2], the assessment of vascular disease [3], structural and functional imaging of the brain [4] and imaging the microvasculature [5, 6, 7]. The technique relies upon irradiating the tissue with nanosecond pulses of low energy laser light. At near infrared wavelengths, due to the relative optical transparency of tissue, the light penetrates deeply (several cm). It is also strongly scattered. This results in a relatively large volume of the tissue becoming "bathed" in diffuse light. Through the processes of optical absorption and thermoelastic expansion, broadband (~30MHz) ultrasonic acoustic waves are excited throughout the irradiated volume and propagate to the surface. Here, as in conventional pulse-echo ultrasound, they can be detected using a single scanning ultrasound detector [4] or an array of stationary ultrasound detectors [1, 2] and spatially resolved to provide a 3D image of the internal tissue structure. Penetration depths of several cm have been demonstrated using near infrared (NIR) excitation wavelengths with mm spatial resolution [2]. For shorter penetration depths of a few mm, higher resolutions of a few hundred microns are achievable [6, 7].

To achieve high resolution imaging based upon the photoacoustic method, high sensitivity (<1kPa), wideband (>20MHz) ultrasound sensors with a near omni-directional response are required. The latter requirement demands that the element size is small (~ tens of microns) compared to the acoustic wavelength. This presents a specific difficulty with piezoelectric receivers due to the reduction in sensitivity that occurs with decreasing element size. The use of a Fabry Perot polymer film ultrasound sensor can overcome this limitation since sensitivity, for a given interrogating laser intensity, is independent of element size which is notionally defined by the dimensions of the illuminating optical beam. In principle, element sizes down to the optical diffraction limit of a few microns are achievable. Previous work has shown that broadband (25MHz) noise equivalent pressures (NEP) of 3kPa are readily achievable [8]. By increasing the finesse of the interferometer and developing a novel high saturation threshold photodiode-amplifier design that enables a much higher interrogating laser power to be used, the detection sensitivity has now been increased by almost an order of magnitude. A sensor with an optically defined element size of 50µm, 20MHz bandwidth and an NEP of 0.35kPa was

* ezzhang@medphys.ucl.ac.uk; phone +44 20 7679 6441

demonstrated and shown to have a sensitivity comparable to that of a PVDF transducer of 1mm diameter active area. This indicated that this type of sensor represents a viable alternative to wideband piezoelectric technology for photoacoustic sensing applications.

2. EXPERIMENTAL SETUP AND OPERATING PRINCIPLES

A schematic of the experimental setup is depicted in Figure 1. The Fabry-Perot (FP) polymer film interferometer comprises a 60μm thick Parylene film with dielectric coatings of reflectivity > 90% at the wavelength of 850nm on its two facets. The sensing structure (including the Parylene film) is vacuum deposited on to a 4 mm thick glass substrate of lateral dimensions 25mm×40mm. The free-space collimated laser beam from an 850nm distributed-Bragg-reflector (DBR) diode laser, which delivers up to 36mW of optical power, is focused down to a small spot size of ~50μm diameter at the FP sensing element — the spot size represents (to a first approximation) the effective active area of the sensor.

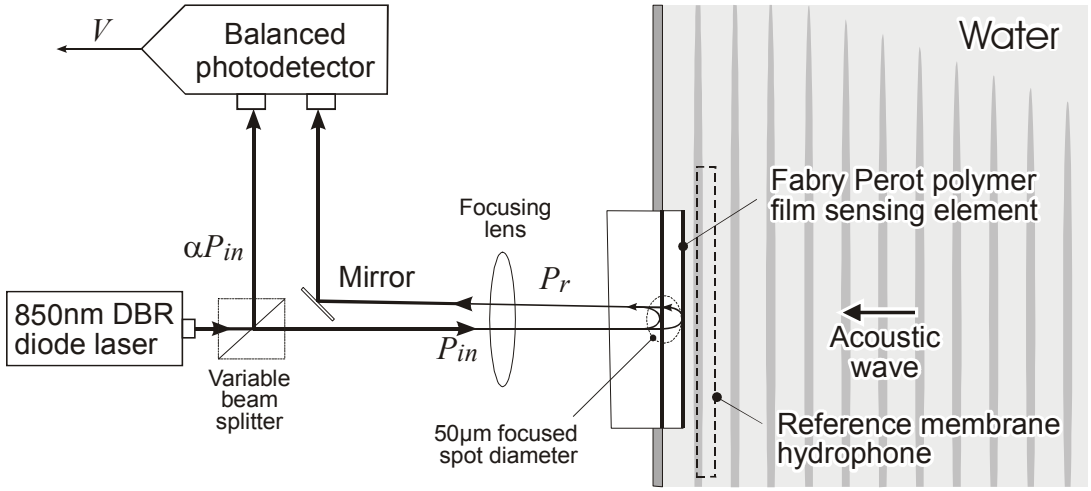

Figure 1: Schematic of the experimental setup. The wavelength of the DBR diode laser is fine tuned by temperature, to set the bias phase, ϕ_0 of the transfer function of the Fabry-Perot interferometer.

2.1. Transduction mechanism of the FP interferometric sensor

The transduction mechanism of the FP interferometric sensor[9] is illustrated in Figure 2. The relationship between P_r, the reflected optical output of the interferometer and ϕ, the optical phase difference between successively reflected beams, is termed the interferometer transfer function (ITF). With an interrogating light source of sufficiently narrow linewidth, the ITF is the product of r, the reflectivity of the FP sensor and the incident interrogating optical power, P_{in} given as

$$P_r = rP_{in} = r(\phi)P_{in} \quad \text{.....(1)}$$

where

$$\phi = 4\pi nd/\lambda \; ; \quad \text{.....(2)}$$

n, the refractive index of the FP cavity media; d, the thickness of the FP cavity; λ, the wavelength of the interrogating light beam. The reflectivity of the FP polymer film sensing element, can be approximated by an expression of the form,

$$r = A + B\left[1 - \frac{1}{1 + (2F_r/\pi)^2 \sin^2(\phi/2)}\right] \quad \text{.....(3)}$$

where F_r is a figure of merit for a FP sensor, termed the reflectivity finesse and referred to as finesse thereafter. A and B are numerical parameters to account for non-ideal factors, such as variation in the polymer film optical thickness, which degrade the visibility, ν defined as,

$$\nu = \frac{\max(P_r) - \min(P_r)}{\max(P_r) + \min(P_r)} \quad \text{.....(4)}$$

The FP sensor described here has a finesse of 17.7 with a measured transfer function as depicted in Figure 2. Its visibility is around 0.67.

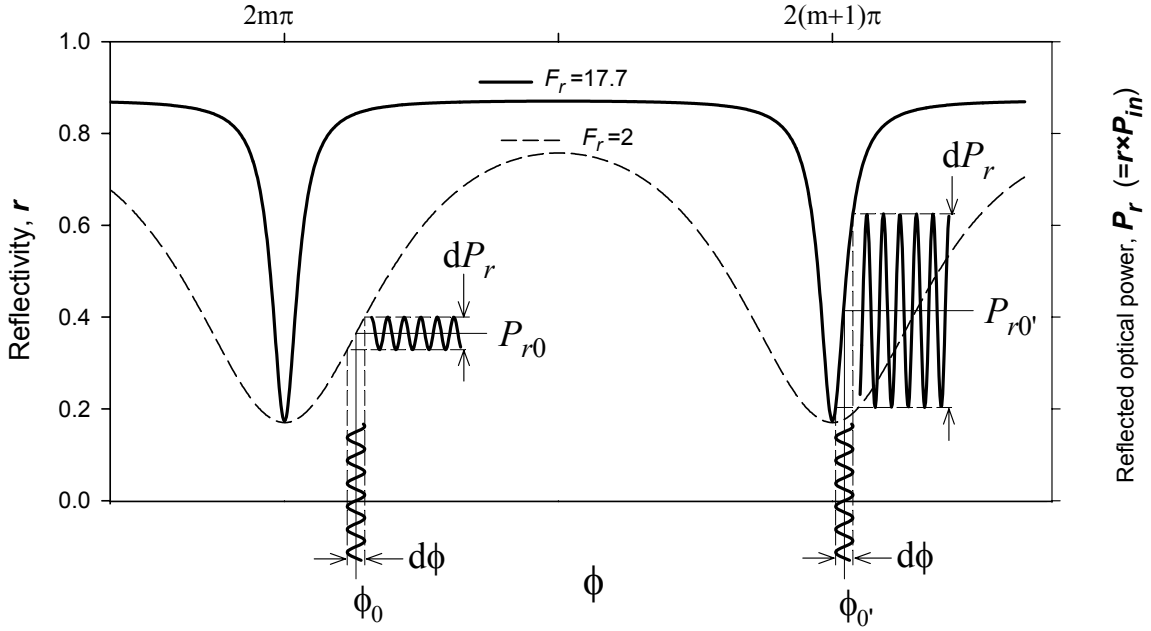

Figure 2: Interferometer transfer function showing optical output P_r of interferometer as a function of ϕ, the phase difference between successively reflected beams. The transfer function for the case of finesse F_r=17.7, depictes the data measured from the FP sensor investigated in this work.

As illustrated in Figure 2, the reflected optical output comprises a constant and a time-varying component, P_{r0} and dP_r, respectively. Consequently, Eq.(1) can be rewritten as:

$$P_r = P_{r0} + dP_r \quad \text{.....(5)}$$

where

$$P_{r0} = r(\phi_0)P_{in} \quad \text{.....(6)}$$

and for a small acoustically induced phase change, $d\phi$

$$dP_r = P_{in}dr = r'(\phi_0)P_{in}d\phi \quad \text{.....(7)}$$

By setting the phase bias ϕ_0 appropriately, the sensitivity of the system can be maximized or optimized with the desired linear range. In this work, ϕ_0 is set by tuning the temperature of the DBR laser diode. As is indicated in Figure 2, the sensitivity can be further increased by employing a FP sensor with a high finesse (hence, a higher value of $\max[r'(\phi)]$) or a higher interrogating power (P_{in}), or both of them.

2.2. Balanced photodetector

In addition to the availability of high power, single mode and narrow linewidth light sources, the maximum interrogating optical power, P_{in} will be limited by the input and output dynamic range of the photodetector employed. For a FP sensor system using a conventional transimpedance photodiode amplifier shown in Figure 3A, the voltage output of the photodetector is given by

$$V = R_f I_{PD} = V_0 + dV \quad \text{.....(8)}$$

where

$$V_0 = R_f S_{PD} r(\phi_0)P_{in} \quad \text{.....(9)}$$

and

$$dV = R_f S_{PD} P_{in} dr = R_f S_{PD} P_{in} r'(\phi_0)d\phi \quad \text{.....(10)}$$

S_{PD} is the photosensitivity of the photodiode; R_f, the transimpedance of the photodiode amplifier. Assuming the maximum positive output swing of the photodetector is $V_{\max}$, the maximum peak-peak value of output voltage change, ΔV is given by

$$\Delta V/2 \le V_{\max} - V_0 \quad \text{.....(11)}$$

Therefore, the maximum interrogating optical power, which can be applied without incurring saturating the photodiode amplifier and signal peak clipping, is given as

$$\max(P_{in}) \le \frac{1}{r(\phi_0) + \Delta r/2} \times \frac{V_{\max}}{R_f S_{PD}} , \quad \text{.....(12)}$$

where

$$\Delta r \approx r'(\phi_0)\Delta\phi \approx r'(\phi_0)\frac{d\phi}{dp}\Delta p , \quad \text{.....(13)}$$

is the peak-peak change of the reflectivity induced by an acoustic wave with a peak-peak pressure of Δp. As is indicated in Eq.(11), the output range of the photodiode amplifier is reduced by the presence of the constant voltage V_0 associated with P_{r0}, the reflected optical power at the bias phase ϕ_0. Reducing the DC voltage, V_0 will increase the output range of the photodiode amplifier and therefore the dynamic range of acoustic pressure measurement. One way to reduce the DC voltage is to lower the feedback resistance, R_f of the transimpedance amplifier and then AC couple its output to a second stage voltage amplifier to compensate for the loss of the transimpedance gain. This approach will degrade the signal-to-noise ratio (S/N) by a certain amount [10], although such degradation will be insignificant at high levels of optical input where the shot noise due to the DC photocurrent dominates.

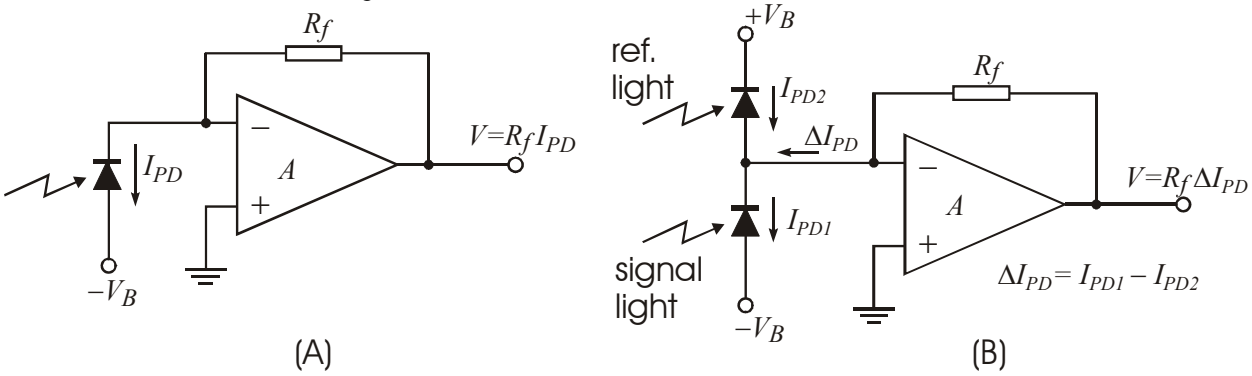

Figure 3: Schematic of photodetectors. (A) Conventional transimpedance photodiode amplifier; (B) Balanced photodetector.

The approach utilized here is to annul the DC voltage, V_0 with the use of the balanced photodetector (BPD) scheme as shown in Figure 3B where the two photodiode used are assumed to be identical. Apart from maintaining the transimpedance gain of the photodiode amplifier, and hence the S/N, the BPD is capable of annulling intensity fluctuations of the interrogation light beam if the reference light is correlated to the interrogating one, e.g. if both of them originate from the same light source. When V_0=0, the BPD is said to be fully balanced. In the sensor system shown in Figure 1, the BPD is in a fully balanced state when its reference input equals the DC part of its signal input, P_{r0}, that is,

$$\alpha P_{in} = P_{r0} \quad \text{.....(14)}$$

where α is the splitting ratio of the beam splitter in Figure 1. At such a state,

$$\Delta V = R_f S_{PD} P_{in} \Delta r \le 2V_{\max} \quad \text{.....(15)}$$

and hence

$$\max(P_{in}) \le \frac{2V_{\max}}{R_f S_{PD} \Delta r} \quad \text{.....(16)}$$

Therefore, comparing Eqs. (15 and 16) to (11 and 12), the annulment of the DC offset, V_0 in the photodiode amplifier will increase the measurement dynamic range of the system as well as the maximum power limit of the interrogating light by a factor of

$$1 + 2r(\phi_0)/\Delta r \quad \text{.....(15)}$$

The output signal amplitude of the sensor system will be increased by the same factor [Eq.(15)] as the interrogating power increases. For a BPD at fully balanced state, its shot noise will be proportional to $\sqrt{2P_{r0}}$. Thus, increasing P_{in} by a factor of $1+2r(\phi_0)/\Delta r$ will improve the S/N of the sensor system by a factor of

$$\sqrt{r(\phi_0)/\Delta r+1/2} \quad \text{.....(16)}$$

in comparison to BPD's single photodiode counterpart shown in Figure 3A. In practice, $r(\phi_0) >> \Delta r$. Therefore, the potential improvement of S/N offered by a BPD is quite substantial provided monochromic interrogating light source with a linewidth narrow enough and adequate output power is available.

3. EXPERIMENTAL RESULTS

3.1. Characteristics of the balanced photodetector

Low noise wideband operational amplifiers (Op amp), CLC425 by National Semiconductor were used in the construction of the BPD shown in Figure 3B. The Op amp has a gain-bandwidth product of 1900MHz and low input voltage noise (1.05nV / √Hz). A number of BPDs have been constructed using various types of photodiodes. Frequency responses of two of these BPDs, Si-BPD #1 and #3, with the photodiodes reversed bias at 12V, were measured when they were in fully balanced states, and are presented in Figure 4. Si-BPD #1 is based on two Centronic's type BPX65 Si PIN photodiodes of 1mm diameter active areas. The two photodiodes utilized in Si-BPD #3 are Hamamatsu's type S5972 Si PIN photodiodes of 0.8mm diameter active area. Both of the BPD can offer a -3dB gain spectrum bandwidth of 35MHz when the CW optical input power (hence the balancing photocurrent I_{PD0}) is low. However, it was found the for Si-BPD #1 the gain bandwidth decreases substantially for balancing photocurrents I_{PD0} in excess of 1mA. It is reduced to ~13MHz when I_{PD0} reaches 10mA, corresponding to 20mW CW optical input at 850nm, as shown in Figure 4. Such a reduction in gain bandwidth is far less significant for Si-BPD #3, and for I_{PD0}=10mA, the gain bandwidth is still greater than 32MHz. Therefore, Si-BPD #3 was used to perform the acoustic measurements described in this work.

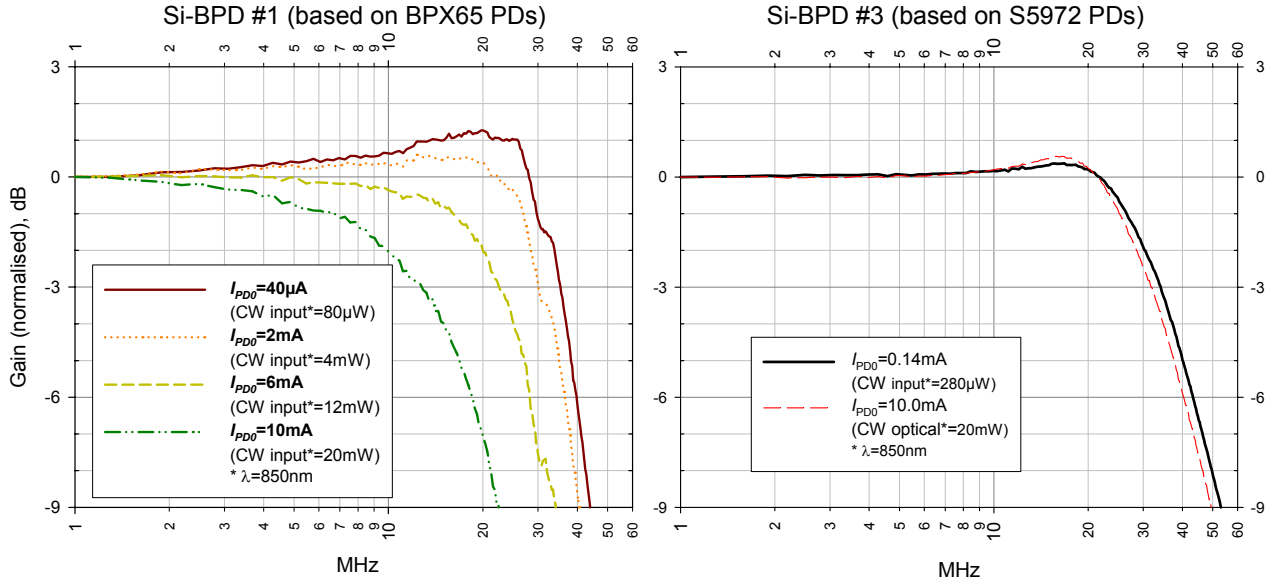

Figure 4: Gain spectrum vs balancing current for two BPDs.

3.2. Acoustic sensitivity measurement

To calibrate the sensitivity of the FP sensor system, a calibrated PVDF membrane hydrophone with a 1mm active diameter was used to provide an acoustic pressure reference. The hydrophone was placed as close as possible to the FP sensor (a few mm apart from each other) as shown in Figure 1 when the reference measurement was taken. The source

of the acoustic wave was a 3.5 MHz planar PZT transducer operating in a repetitive pulse mode and positioned ~250mm away from the FP sensor.

Figure 5 illustrates temporal graphs of acoustic pulses (9 kPa p-p) measured by the FP sensor with the optical power incident on the FP sensor slightly exceeding 20mW and a commercially available 1mm diameter PVDF (28μm thick) needle hydrophone, respectively. The PVDF needle hydrophone has a high performance preamplifier positioned only ~5cm away from the PVDF element to minimize cable loading. Its S/N performance is considered to be representative of state-of-the-art PVDF sensors.

Data for graphs in Figure 5 was acquired by a digital oscilloscope with the measurement bandwidth set at 20MHz. The shape of the waveform captured by the FP sensor, shown in graphs A, was found to be in close agreement with that of the reference membrane hydrophone which has a near uniform frequency response. Unlike the FP sensor (which also has a flat frequency response over its operating frequency range [9]), the needle hydrophone exhibits a significant peak in its response over the region 0.5 – 5 MHz, resulting in the third distinctive peak revealed in graph B.

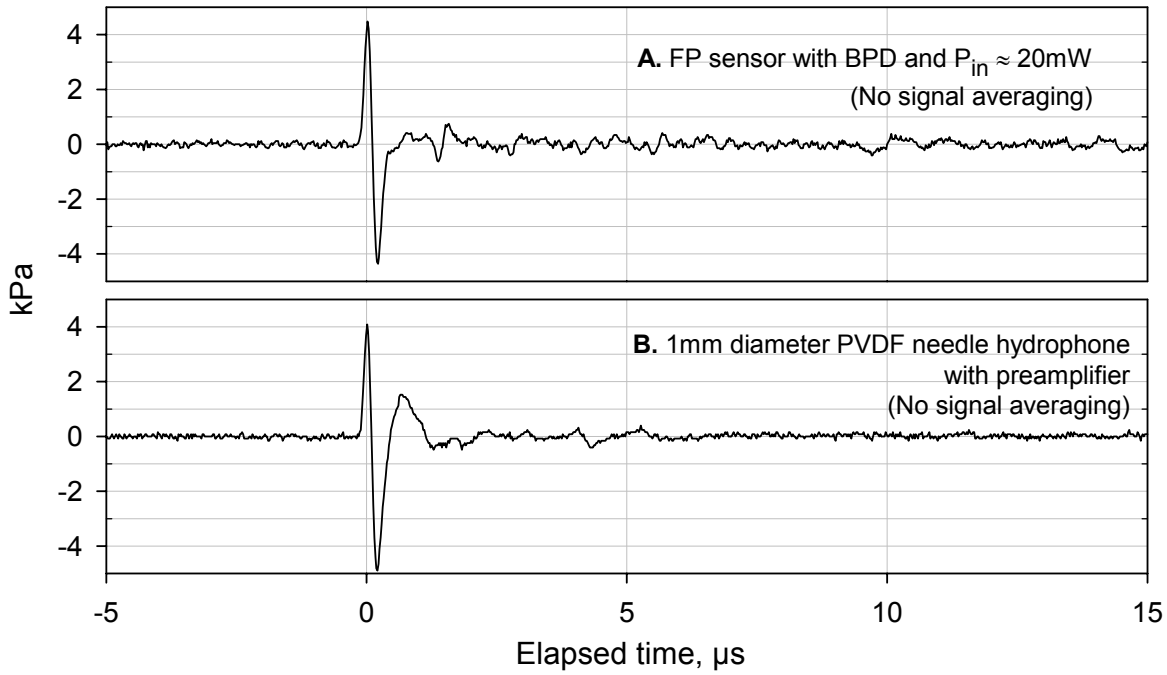

Figure 5: Measurements of an acoustic pulse (9kPa p-p) by the FP sensor and PVDF detector.

Graphs A and B in Figure 5 are measurements taken without signal averaging. The portion before the arrival of the pulse represents the background noise of the corresponding acoustic sensing system. These graphs illustrate that for P_{in} = 20 mW, the signal-to-noise ratio (S/N) of the FP acoustic sensor is comparable to that of the 1mm diameter PVDF needle hydrophone. The noise equivalent or the minimum detectable pressure (NEP) is around 0.45 kPa peak-peak (p-p) for the former and 0.33 kPa p-p for the latter, over a measurement bandwidth of 20MHz.

Experimental measurements of the peak-peak signal output of the BPD and background noise when measuring a 41.5 kPa p-p acoustic pulse without signal averaging, for various power levels of interrogating light at 850nm are depicted in Figure 6. The noise level measured, in the absence of the acoustic pulse, is presented in the upper graph, where the dashed line represents the calculated shot-noise due to the balancing photocurrent. The calculation of S/N shown in the lower graph is based the peak-peak values of the output signal and background noise.

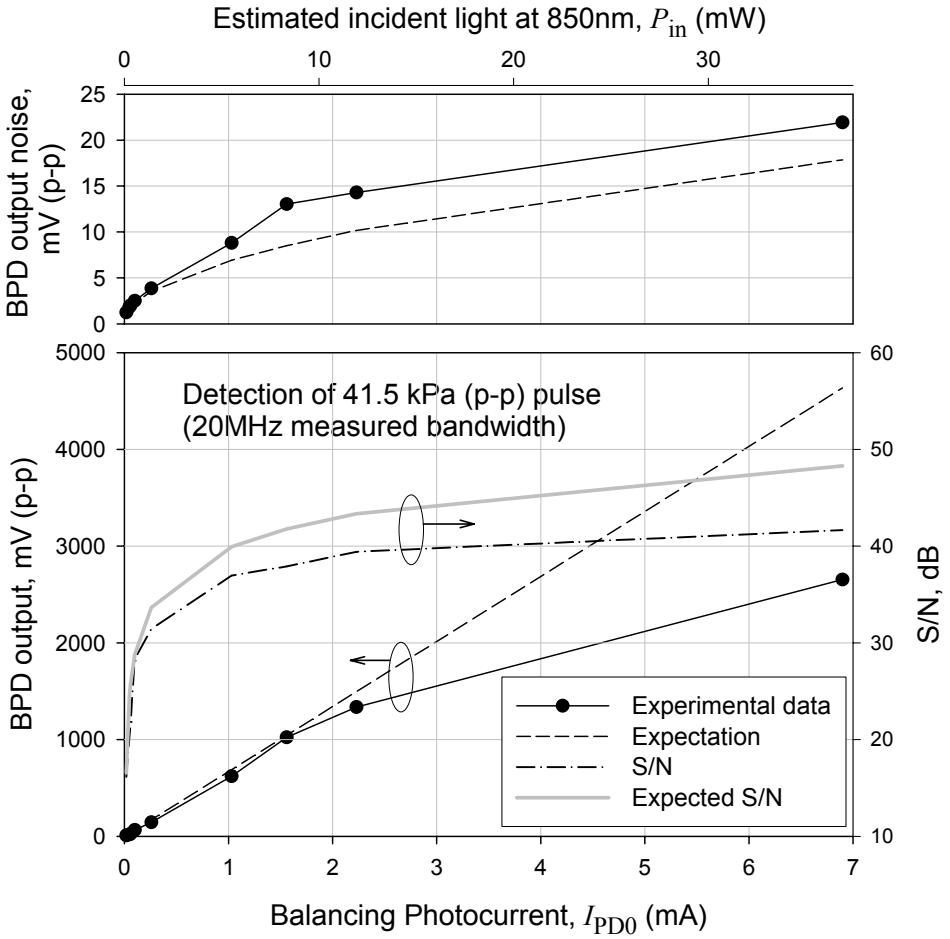

Figure 6: Output signal and noise of the BPD when the FP sensor system is measuring an acoustic pulse of 41.5kPa (p-p), for various power level of interrogating light at 850nm.

The BPD output amplitude is expected to increase linearly with the increase of interrogating light power, as shown by the dashed line in the lower graph in Figure 6. However, as Figure 6 shows, for P_{in} > 10 mW, the sensor signal amplitude does not appear to scale linearly with P_{in}. This is thought to be due to the drift of the phase bias of the FP sensor during the experiment. There are two possible reasons for this. One is the drift of the wavelength of the interrogating light moving the bias phase shown in Figure 2 from the optimum point. The other is that localized heating generated by focusing the high intensity interrogating light beam, raises the temperature at the interrogated spot and hence changes the optimum phase bias point. Nevertheless, a high S/N of 42 dB was achieved when the interrogating power was raised to ~36mW, which corresponds to a minimum detectable pressure of 0.35kPa. With the use of a laser source with sufficient tuning range and speed to enable the tracking of the phase bias drift, the high sensitivity represented by the dashed line in the lower graph of Figure 6 could be achieved. The FP sensor system would then provide a S/N of 48 dB, which corresponds to a minimum detectable pressure (p-p) of 0.16 kPa. For a FP sensor system with a conventional transimpedance photodiode amplifier in a similar setup, the minimum detectable pressure would be 2 kPa.

4. CONCLUSION

A high sensitivity, wideband ultrasound sensor based on a high finesse FP polymer film interferometer has been demonstrated with a bandwidth of 20 MHz and an active area of less than 50μm diameter. Used in conjunction with a balanced photodetector to enable the use of high intensity interrogating light beam up to 36mW, the sensor system

provided an NEP of 0.35kPa over a 20 MHz measured bandwidth. The S/N performance or sensitivity of the FP sensor is comparable to that of a 1mm diameter PVDF detector. Based on the experimental data for interrogating optical power less than 10mW, the NEP could be reduced to less than 0.16 kPa (instead of the measured 0.35 kPa) by increasing the power to 36mW and using a laser with sufficient tuning range and speed to maintain the optimum phase bias point..

For photoacoustic imaging applications, the repetitively induced acoustic signal can be mapped by scanning the interrogating light beam across the FP sensing film. In practice, due to the unevenness of the film thickness and other imperfections in the sensor, the transfer function may vary significantly from one interrogated point on the sensing film to the other. Hence, the optimum phase bias will vary accordingly. This requires rapid adjustment of the phase bias. An angle tuning method has been successfully demonstrated for controlling the phase bias of a low finesse FP sensor based photoacoustic imaging system [6, 11]. However, for high finesse FP sensors, this can lead to a degradation in fringe visibility due to the non normal angles of incidence. Under these circumstances, wavelength tuning of the phase bias is preferred as normal incidences that are encountered can be maintained to provide optimum sensitivity. The increase in the ITF visibility can also lower the reflected DC light P_{r0} and reduce the balancing current (and hence the shot-noise). Compared to tunable laser sources at 850nm, high power, widely and rapidly tunable lasers operating in the 1550nm band developed for telecommunications are available at relatively low cost. These attributes indicate that they may be more suitable interrogating light sources for the FP sensor.

ACKNOWLEDGEMENT

This work is sponsored by the Engineering and Physical Science Research Council, UK.

REFERENCES

1. Kruger R.A., Miller K.D., Reynolds H.E., Kiser Jr W.L., Reinecke D.R. and Kruger G.A., Contrast enhancement of breast cancer in vivo using thermoacoustic CT at 434 MHz, Radiology, 216, pp.279-283, 2000

2. Andreev VG, Karabutov AA, Solomatin SV, Savateeva EV, Aleynikov V, Zhulina YV, Fleming RD, Oraevsky AA, Optoacoustic tomography of breast cancer with arc-array-transducer, Proc SPIE Vol 3916, pp36-47, 2000

3. Paul C Beard and Mills T.N, Characterisation of *post mortem* arterial tissue using time-resolved photoacoustic spectroscopy at 436nm, 461nm and 532nm, *Physics in Medicine and Biology*, Vol 42, No 1, pp177-198, 1997.

4. X Wang, Y Pang, G Ku, X Xie, G Stoica and L Wang, "Noninvasive laser-induced photoacoustic tomography for structural and functional *in vivo* image of the brain," Nature Biotechnology, 21 (7), pp.803-806 (2003).

5. Hoelen CG, de Mul FFM, Pongers R, Dekker A, , Three-dimensional photoacoustic imaging of blood vessels in tissue, Optics Letters, Vol 23, No 8, pp648-650, 1998

6. Paul C Beard, Photoacoustic imaging of blood vessel equivalent phantoms, Proc. SPIE, Vol. 4618, pp.54-62, 2002.

7. Magdalena C. Pilatou, Nico J. Voogd, Frits F. M. de Mul, Wiendelt Steenbergen, and Leon N. A. van Adrichem, Analysis of three-dimensional photoacoustic imaging of a vascular tree in vitro, Rev. Sci. Instrum. 74, pp.4495-4499, 2003.

8. Beard PC and Mills TN, A 2D optical ultrasound array using a polymer film sensing interferometer, Proc. IEEE Ultrasonics Symposium 2000, pp.1183-1186, 2000.

9. Paul C Beard, Frederic Perennes and Tim N Mills, "Transduction mechanisms of the Fabry-Perot polymer film sensing concept for wideband ultrasound detection," IEEE Trans. Ultrasonic, Ferroelectric, and Frequency Control, Vol. 46 (6), November 1999.

10. "Designing photodiode amplifier circuits with OPA128", Application bulletin, Burr-Brown Corporation (1994)

11. P C Beard, "Interrogation of free-space Fabry-Perot sensing interferometers by angle tuning," Measurement Science and Technology, **14**, pp.1998-2005 (2003)